ELSEVIER

Contents lists available at ScienceDirect

## **Applied Energy**

journal homepage: www.elsevier.com/locate/apenergy





# Opportunities of in situ diagnostics and current distribution in proton exchange membrane water Electrolyzers with segmented bipolar plates

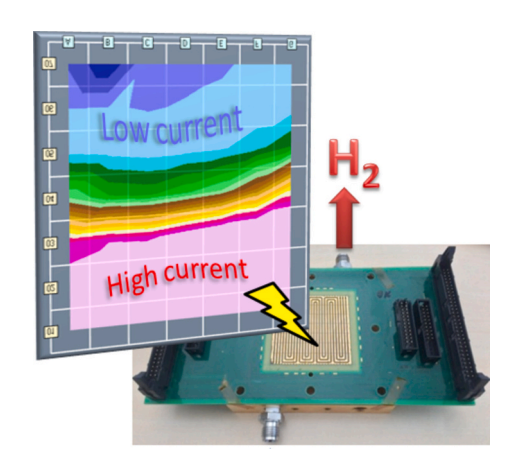
Benjamin Kimmel<sup>a</sup>, D. Garcia-Sanchez<sup>a,\*</sup>, T. Morawietz<sup>a</sup>, M. Schulze<sup>a</sup>, I. Biswas<sup>a</sup>, A.S. Gago<sup>a,\*</sup>, K.A. Friedrich<sup>a,b</sup>

- a Institute of Engineering Thermodynamics, German Aerospace Center, Pfaffenwaldring 38-40, Stuttgart 70569, Germany
- b Institute for Building Energetics, Thermotechnology and Energy Storage, University of Stuttgart, Keplerstraße 7, Stuttgart 70174, Germany

#### HIGHLIGHTS

- In-situ diagnostic tool for PEM electrolyzers
- Segmented bipolar plate for monitoring the state of health of PEM electrolyzers
- Versatility of the segmented bipolar plate for studying gas removal/water supply, inadequate flow field designs in the bipolar plate and mass transport losses at high current densities
- Advantage of the segmented bipolar plate for studying local degradation effects
- Segmented bipolar plate combines insitu diagnosis and on-line regulation

#### GRAPHICAL ABSTRACT



## ARTICLE INFO

Keywords:
PEM electrolysis
Segmented cell
Degradation
Current density distribution
In situ analysis

#### ABSTRACT

The widespread implementation of renewable energy for the decarbonization of our society is a pressing challenge that requires the use of large-scale electrolyzers to produce green hydrogen. Proton exchange membrane water electrolysis (PEMWE) is ideal for this purpose given its small footprint and flexibility to operate dynamically. However, little is known about the degradation of PEMWEs, and advanced techniques are required for monitoring the health states of stacks. Here, we have successfully integrated a powerful tool for in situ diagnostics in a 25 cm² active area PEMWE. A segmented bipolar plate (SBPP) allows local measurements of current and temperature. A series of experiments showing the benefits of the SBPP are described in this work. First, clamping pressure due to uneven torque forces can be determined with the SBPP during cell assembly. When varying the temperature to 80 °C, the current distribution in the cell area is homogeneous over the cell area. Conversely, the tool reveals local current differences reaching 80 % when limiting the water flow in the catalyst-coated membrane (CCM). Furthermore, mass transport phenomena due to flow field design are nonuniform over the cell area and can be monitored at current densities approaching 5.5 A cm². Finally, SBPP is used to investigate local degradation due to contaminants, showing different deactivation zones of the electrode

E-mail addresses: daniel.garciasanchez@dlr.de (D. Garcia-Sanchez), aldo.gago@dlr.de (A.S. Gago).

<sup>\*</sup> Corresponding authors.

due to poisoning, which is confirmed by energy dispersive X-ray spectroscopy (EDS). The SBPP is versatile and robust, and it opens the possibility for studying in situ a wide range of cell phenomena from mass transport to degradation, thus demonstrating its superior value for diagnostics in PEMWE systems in many different research fields

#### 1. Introduction

In recent years, global warming due to climate change has reached a critical point. Anthropogenic CO2 is one of the major greenhouse gases causing atmospheric warming and sea acidification. Therefore, the decarbonatization of our society is a pressing challenge. The European Union enacted pathways to reach carbon neutrality by 2050 [1]. The widespread deployment of renewable energies is mandatory to achieve these goals. In recent years, the share of renewable energy has increased significantly. The maximal electrical capacity of wind and photovoltaics in the European Union (U-27) has increased from 140 GW in 2011 to 315 GW in 2020 [2]. In Germany, 19.7 % of gross final energy consumption is already covered by renewable energies in 2021 [3]. In terms of renewable energy, wind turbines and solar photovoltaics offer the highest technical potential to produce clean energy [4]. The drawback of these technologies is the variable, weather-dependent amount of produced electricity. Due to these fluctuations, grid balancing is mandatory. Rather than curtailment, storing excess energy is a better approach for grid balancing to yield a higher net energy return [4]. In this context, there is greater interest in hydrogen as a secondary energy carrier that stores chemical energy [5]. In addition, hydrogen can be easily transported in different ways, thus representing a key component in future energy systems [5]. Proton exchange membrane water electrolysis (PEMWE) is a promising technique to produce green hydrogen from renewable energy. The rapid response time and wide operation range make PEMWE systems highly suitable for coupling with renewable energy sources [6,7]. Furthermore, high efficiencies, high power densities, compact design and superior gas quality are other advantages of PEMWE systems [6,8-10]. To fulfill climate goals, electrolyzer plants on a megaor even gigawatt scale are needed. The European Union set up targets to build a 6-GW electrolyzer until 2024 and two 40-GW electrolyzers until 2030 [1]. However, the upscaling of PEMWEs is recently hindered by the high investment costs of stack components [6].

Due to the corrosive environment and high operating voltages, titanium bipolar plates (BPPs) are mainly used in PEM cells [6,10,11]. In addition to titanium plates, the required precious metal content contributes noticeably to the overall cost. Thus, recent research is focusing on the cost reduction of PEMWE stacks. The harsh environment makes it necessary to gain knowledge of degradation behavior and prove lifetime when studying new materials [6]. Therefore, the need for diagnostic and in situ characterization tools is increasing. The operando measurement of the local current density represents an important part of the assessment of the performance and durability characteristics of new materials [12].

The measurement of the current density distribution (CDD) is a common practice in proton exchange membrane fuel cells (PEMFCs). Segmented cell, which is the device for in situ measurement of the local CDD, have established themselves as a powerful diagnostic tool in PEMFCs. An early utilization of segmented cells for PEMFCs has been reported by Cleghorn et al. [13]. In recent years, several studies of local processes have been carried out [14–20]. The research conducted with the segmented cell is crucial to understand some of the key problems toward the widespread deployment of PEMFC technology. Essential knowledge has been gained over the years in research fields, such as water management [21–25], contamination/durability [26–29] and fuel starvation [28,30–32]. There are several techniques for determining local current density; however, SBPP with printed circuit boards (PCBs), which are patented by the German Aerospace Center (DLR) [33,34], are the most favorable because of their ease of use and suitability for single-

cell and commercial fuel cell stack applications [19]. In addition to its functions as an in-situ characterization and diagnostic tool, SBPP has the potential to act as a monitoring tool. Lin et al. showed through their study on the evolution of leakages that malfunctions can be detected at early stages. Therefore, by using SBPP as an online monitoring and feedback tool, catastrophic failures of the whole stack [20] and unfavorable conditions may be avoided [19]. SBPP yields valuable information to study and evaluate the influences of cell components, such as a GDL, a membrane and catalyst layers on the performance [35–38].

The current density distribution measurement is of great interest in PEMWE; however, various challenges need to be considered for the implementation of SBPP in PEMWE. The device has to be adapted to endure high current densities. SBPP gaskets must maintain tightness even under high water and gas pressure levels. Cell voltages above 2 V and the corrosive environment due to the acidity of the membrane and the high concentrations of dissolved  $O_2$  and  $H_2$  result in pronounced electrochemical stresses and therefore high demands on durability [12,39]. For in situ measurement, the influences of the SBPP on the performance and durability must be reduced to a minimum. Thus, the design and properties of the SBPP should be as close as possible to those of the replaced BPP [12].

In their review of degradation studies and operating conditions, Wallnofer-Ogris et al. emphasised the importance of electrochemical analysis methods such as segmented cells [40]. There are a few works on measuring local current density; however, development is still at an early stage. Merwe et al. showed the general functionality of current density mapping in PEMWE by adapting a fuel cell setup [41]. Dedigama et al. combined one-dimensional current mapping with flow visualization [42]. Sun et al. investigated the drying behavior of a single cell with an integrated segmented MEA [43]. Immerz et al. performed similar experiments with a single channel setup [44,45]. The influences of different flow field designs and pressure distributions on the current density distributions were investigated by Minnaar et al. [46] and Verdin et al. [47]. Shakhshir et al. investigated the effect of different clamping pressures, while Parra-Restrepo et al. studied the effect of different porous transport layers (PTL) on the current density distribution [48,49]. An investigation of mass transport limitations for different flow fields and diffusion medias using segmented cell technology was carried out by Roenning et al. [50]. A long channel cell setup for locally resolved current density measurements was developed by Hensle et al. to investigate high current densities and high temperatures [51]. Wang et al. investigated in-plane temperature and current heterogeneity under different conditions [52].

In this work, the SBPP is implemented in a PEMWE to measure local current density and temperature distribution. The results of this study provide new insights into the CDD with local resolution and dependencies on clamping pressure, temperature, mass transport limitations and degradation phenomena.

#### 2. Experiment

#### 2.1. Segmented bipolar plate (SBPP) design

To visualize the homogeneity of the CDD, locally resolved current density measurements are performed using a PCB as the SBPP with an integrated flow field in the cathode. Fig. 1a) shows an image of the PCB that was used for all the measurements. The PCB has an area of  $50.2 \times 50.2 \text{ mm}^2$  and is divided into 49 segments for current measurement. Fig. 1 b) shows the labeling of the segments. In addition, the measuring

board has six integrated temperature sensors suitable for 120 °C. The sensors are distributed on the surface as depicted, and they are labeled T1, T2, T3, T4, T5 and T6 in Fig. 1b). To avoid lateral conductivities between the segments, the board is made of nonconductive material. Each segment is covered with a conductive Cu-upper layer and is separately connected to the rear layer via conductive wires and a calibrated resistor. By measuring the voltage drop at the resistors, the current flow through each segment can be determined separately. The PCB has an integrated 3-channel serpentine flow field. Therefore, the PCB can directly replace the BPP on the cathode side, as shown in Fig. 1a). Gold coating the Cu segments reduces the corrosion of SBPP. An example of a false color plot visualizing the CDD measured using a SBPP and the corresponding color code is illustrated in Fig. 1 c) and d), respectively. Notably, segment B7 of the segmented board isn't working properly, therefore measuring wrong current values. This leads to deviation in the false color plots also in the neighboring segments, as the plots uses an interpolation to show smooth, more intuitive gradients between individual segments. By acknowledging this local deviation and focusing on the other segments and the overall characteristics of the current density distribution, measurements can still be evaluated and conclusions drawn without negatively impacting the measurement campaign of this work. In order to demonstrate the capability of upscaling to larger electrolyzers, a SBPP was implemented in a commercial stack. Fig. 1 e) shows the printed circuit board attached to the backside of the BPP.

#### 2.2. Cell configuration and electrolyzer tests

An in-house produced cell was used for investigation. The cathode end plate was produced of stainless steel (ss314). To prevent corrosion, the end plate was provided with a necessary Ni precoat layer and gold coated by electrodeposition. The SBPP was on the cathode end plate. The porous transport layer (PTL) on the cathode side was 280-um carbon paper (Toray). The PTL ensured homogenous electrical contact and provided good water and gas transport. A commercial CCM with an active area of 25 cm<sup>2</sup> was used. The anode and cathode catalysts of the Nafion 115-based CCM were Ir and Pt/C, respectively. Due to the harsh environment on the anode side, a 1 mm thick sintered titanium plate (GKN) was used as the PTL. The anode end plate with an integrated flow field was varied to study the impacts of different flow fields. In this paper, a Ni/Au-coated 5-channel serpentine flow field and a Ti-coated parallel flow field were investigated. The measurements with the segmented cell were compared with standard hardware used in the German Aerospace Center. By comparing the polarization curves from previous and this work in Supplementary S1 a negative impact on performance was not observed. [53,54]

The experiments were performed with an in-house built test bench. The test bench was equipped with adjustable water circulation for the anode side. The cathode side was kept dry while the inlet remained closed. The cell temperature was controlled and varied by the temperature of the inlet water. Ion exchange resin that was integrated in the water circuit before the cell warranted water resistance values above 10

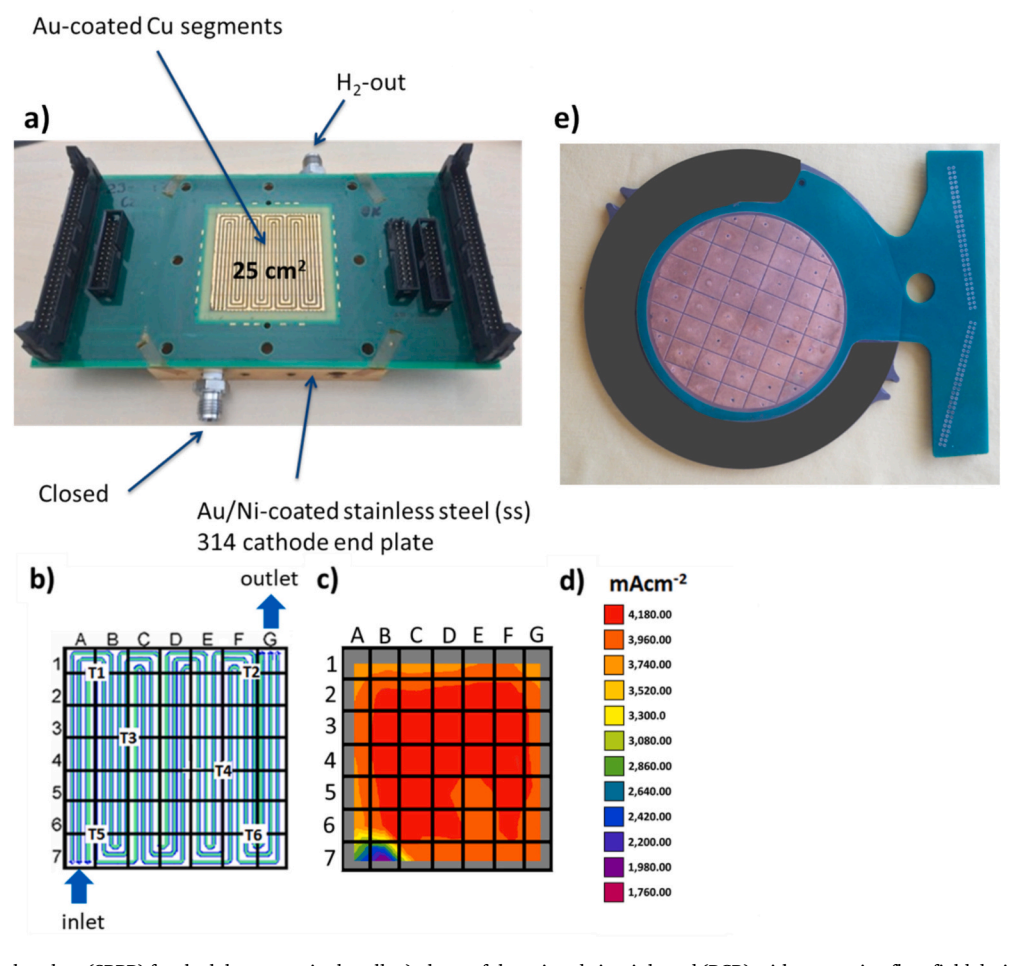


Fig. 1. Segmented bipolar plate (SBPP) for the laboratory single cell: a) photo of the printed circuit board (PCB) with serpentine flow field design; b) segmentation; c) current density distribution chart and d) color code for current density values. The inlet and outlet of the feed water is indicated with blue arrows. Segmented bipolar plate for stack validation: e) photo if the printed circuit board attached to the backside of the BPP. (For interpretation of the references to color in this figure legend, the reader is referred to the web version of this article.)

 $\rm M\Omega$ . Polarization curves were obtained with a scan rate of 4 mAcm<sup>-2</sup> s<sup>-1</sup>. To determine the resistance values within the cell, electrochemical impedance spectroscopy (EIS) was measured using an IM6 setup with a Booster P240 (Zahner-Electrik). The measuring range was set to 10 kHz to 100 mHz for different current densities and adjusted amplitudes. The data acquisition unit connected to the SBPP recorded the current density and temperature distribution every five seconds. Unless otherwise mentioned, an anode end plate with a parallel flow field was used.

To demonstrate the advantages of using SBPP, several experiments were carried out showing the behavior of the CDD under certain conditions and the versatility of the system to the reader. To investigate the phenomena of each experiment separately, pristine cells we assembled and used for each experiment. In the following section, we will describe these experiments: the advantage of the SBPP in controlling the compression force, the influence of the operation condition, the influence of the cell component design and the local degradation effects. In the first experiment, the impacts of clamping pressure on local current densities were investigated. Therefore, the initial torque of the selected screws was reduced to 0.5 Nm, while the others were tightened to 2.2 Nm. A 5-channel serpentine flow field on the anode side was used for this experiment. The cell temperature was maintained 60 °C. All experiments were performed at 1 bar. The impacts of the cell temperature on the CDD were investigated at 30, 50, 65 and 80 °C. High gas production rates could lead to insufficient water supply to the active sites of the CCM. To simulate and investigate this effect, the water input valves were closed after maintaining a stable state at 70 °C. This routine was repeated for 5 different currents. To enable a direct comparison of the impacts of different flow fields on the CDD, experiments were carried out with the same operating conditions, and only the anode flow field was exchanged. Further experiments were performed with current densities reaching 5.5 A cm<sup>-2</sup> at cell temperatures of 80 °C. Finally, a degradation experiment was conducted. Therefore, the cell with the 5channel serpentine flow field was operated for three days without refreshing the water and with ion exchange resin filters removed to intentionally poison the membrane.

The validation experiments for industrial stacks were carried out using PEMWE hardware by EWII Fuel Cells (continued by Green-Hydrogen.dk). A prototype SBPP of spherical geometry, with 44 segments of rectangular and, in the edge regions, partially rectangular shape, was designed for this electrolyzer. The SBPP was embedded in a 3-cell short-stack of 76.5 cm<sup>2</sup> between the first and second cells. The circulating water supply and the stack itself were preheated to 45 °C. With the exception of these modifications and some extended tubing to provide space for the prototype SBPP, the system was not modified. The load was controlled by ramping the current with the integrated control system. A specific scenario of the local deactivation of the electrolysis process was mimicked by interrupting the feed water supply directly before the automated start-up of the system. While the industrial hardware was designed to self-pressurize to 50 bars, the experiments were carried out with 2 bars. The local current densities were recorded with a modified data acquisition unit to match the specifications of the SBPP prototype. The achievable frame rate for the prototype was  $\sim 0.19$ frames/s.

#### 2.3. Postmortem analysis

For elemental analysis, EDS spectra were taken at both electrodes and at different positions at the membrane, in the center and close to the electrodes, with a Jeol JSM-7200F SEM combined with a Bruker Quantax EDX detector. To assess the distribution of Ni in the CCM, at each sample, three line scans were performed by scanning across the CCM from the anode to the cathode. The measuring time was set to 600 s in total for 100 points. The Ni content was evaluated by Bruker software (Esprit), considering all detected elements.

#### 3. Results and discussion

#### 3.1. Clamping pressure during cell assembly and operation

Stack assembly is a key step in the industrial production of PEMWE. BPPs, PTLs and CCMs must adhere to small tolerances in thicknesses to maintain a homogeneous contact pressure over the cell area. However, if the thicknesses of the components are not homogenous and if the torques of the bolts and nuts are not adjusted to compensate for this, nonuniform contact pressure can lead to losses in performance and durability. Thus, SBPP can be used to monitor clamping pressure during cell assembly and operation. First, the CDD is measured during stable operation when all bolts and nuts are clamped with an initial torque of 2.2 Nm. The current mapping is shown in Fig. 2a) and is evenly distributed over the whole surface. The torque reduction in a single bolt does not have a noticeable impact on the CDD, and three bolts are sufficient to keep the clamping pressure uniform. In Fig. 2b), the torques of the two bolts are set to 0.5 Nm, as represented by green circles. This result leads to a current density drop on the upper part of the cell; a higher current is measured in the lower part than the upper part. The reason for this redistribution within the cell can be assigned to the poor electrical contact due to lower clamping pressure [47]. Thus, with the help of CDD, spots with less clamping pressure can be localized. Especially in stacks, it is complicated to detect screws with less torque. SBPP as an in situ diagnostic tool can help to detect low clamping pressure after assembly and online during operation and help to assure high quality of production.

#### 3.2. Current, temperature, water distribution and starvation

The electrical current and the corresponding cell voltage, temperature and water supply are the main factors that influence PEMWE cell performance. Temperature has noticeable impacts on the performance of electrolysis cells [55,56]. To study the CDD at different temperatures, four polarization curves at 30, 50, 65 and 80 °C are measured, and the results and current density mapping at 1 Acm<sup>-2</sup> for each curve are shown in Fig. 3. Through the polarization curves in Fig. 3 a), a temperature increase reduces voltages and therefore improves the performance of the PEMWE. To reinforce the study of the influence of temperature on performance, EIS measurements are carried out. From the Nyquist plot at 0.5 Acm<sup>-2</sup>, displayed in the inset of Fig. 3 a), one can observe how the left intersection with the x-axis shifts left when the temperature is increased; the width and height values of the curves remain constant. While the interpretation of semicircles in the EIS measurements in PEMWE devices is controversial, the first intercept is commonly attributed to ohmic resistance values [57,58]. Increasing the temperature leads to a more homogeneous current density distribution, especially the outer regions of the cell area, which show a higher and more even current density, as shown in Fig. 3 b). Therefore, the use of the SBPP allows statements to be made about the performance based on CDD at local and global scales.

Water shortages due to pump failure are rare in commercial electrolyzers, and water contamination is the main reason for failure in PEM electrolysis [59]. Nevertheless, failure of the control system is a problem that should be considered, as it may lead to insufficient water in the electrolyzer system. In addition, the following experiment can simulate insufficient water supply to the active sites of the CCM due to high gas production rates. A large amount of gas bubbles on the catalytic surface might hinder a uniform water distribution over the area of the CCM caused by extremely high current densities, inappropriate flow field designs and small PTL pore sizes. This phenomenon is especially critical for stacks with large active areas, such as those used in Cummins Inc. [60] or Siemens [61] electrolyzers.

Moreover, pumps for such large systems consume considerable energy and are costly. Ideally, the stacks should be operated via natural flow; however, in this case, there will be a high amount of produced gas

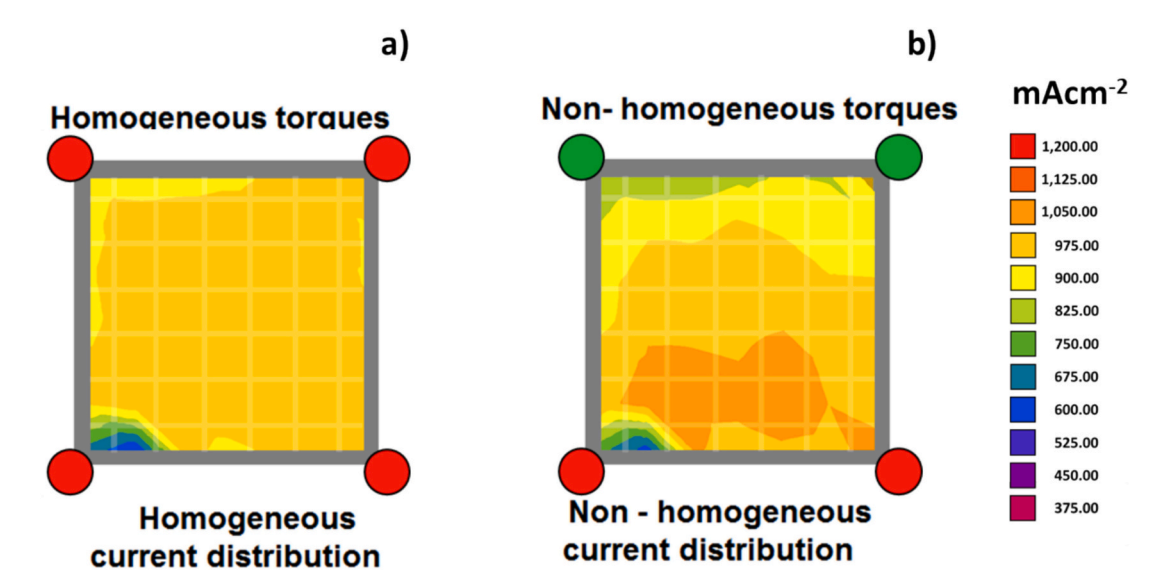
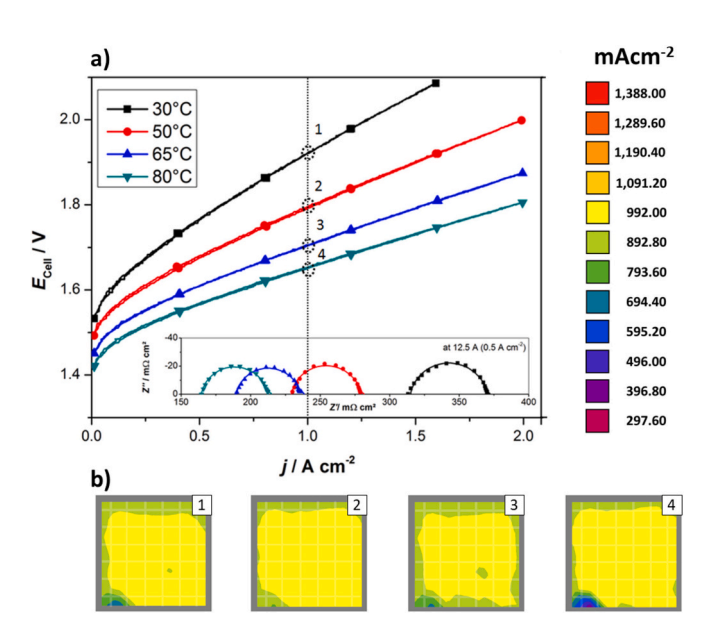


Fig. 2. Effects of applying torque a) homogenously and b) nonhomogenously during cell assembly in the current distribution chart. The corresponding color code scale of current density is shown on the right. Anode flow field: 5-channel serpentine flow field. Cathode flow field: 3-channel serpentine. The feed water enters at the bottom left and exits at the top right on the cathode side.



**Fig. 3.** a) Cell voltage ( $E_{cell}$ ) vs. current density (j) characteristics recorded at 30 °C, 50 °C, 65 °C (nominal) and 80 °C. The inset shows the Nyquist plots of the EIS at 0.5 Acm<sup>-2</sup>. b) The current distribution charts at 1 A/cm<sup>2</sup> for the different temperatures are shown with the corresponding color code current density scale on the right. Anode flow field: parallel. Cathode flow field: 3-channel serpentine. The feed water enters at the bottom left and exits at the top right on the cathode side.

in the cells and insufficient water replenishment to the electrodes. Thus, the segmented cell can be useful to determine the optimal overall current density to avoid heterogeneity in the local current density distribution.

For the following experiment, the electrical pump is shut off while the load is still applied to simulate the situation with limited water supply. Fig. 4 a) shows the change in voltage during the course of the experiments. The effects of water starvation on the CDD are presented in Fig. 4 b). The direction of gravity is indicated by the arrow. When closing the water inlet at time 1, marked in Fig. 4 a), the current mapping for all different currents is largely evenly distributed seen in Fig. 4 b). Low current densities are depicted in purple/blue while they rise

through green, yellow and end in orange/red at the highest current densities. Due to the reduced water consumption at low currents, especially at  $0.8 \,\mathrm{A\,cm^{-2}}$  (20 A), stable operation can be maintained for a relatively long period. If the amount of water reaches a critical low value, water starvation begins, which leads to uneven water distribution within the cell. Time 2 in the diagram indicates the start of the voltage increase due to water starvation. The current mappings at point 2 show rather heterogeneous distributions, which are more pronounced at high currents. Above 2.4 A cm<sup>-2</sup> (60 A), the current densities decrease in the lower parts of the CDD plots, while the current densities increase in the upper parts. This phenomenon is due to the gravitational effect. The remaining water in the cell flows in the direction of gravity. Due to the orientation of the CDD plots, the water accumulates in the upper part of the diagrams. As a result, in the area with high water content, high current densities occur. This effect intensifies drastically at time 3, and the voltage starts to increase almost vertically. This experiment demonstrates the functionality of SBPP as an in situ diagnostic tool to measure and recognize changes in the water supply over the CCM. In combination with appropriate control strategies, degradation and even catastrophic failure can be avoided.

#### 3.3. Mass transport and high current densities

In this experiment series, the impacts of different flow fields, high current densities and mass transport phenomena on the CDD are investigated. The polarization curves of two different flow fields are shown in Fig. 5 a). A 5-channel serpentine flow field and a parallel flow field are used on the anode side. On the cathode side, an SBPP with a 3channel serpentine flow field is used. The empty squares and the CDD charts on the top are the measurement results for the serpentine flow field. The CDDs are recorded at 1 A cm<sup>-2</sup> in 1) and 3) and at 2 Acm<sup>-2</sup> in 2) and 4). The polarization curve using the parallel flow field shows a significantly better performance. Furthermore, in contrast to the serpentine flow field, the parallel flow field does not show hysteresis. In addition, the CDD of the parallel flow field is more homogenously distributed. This finding indicates the presence of mass transport losses in the case of a serpentine flow field. This result is in good agreement with the reports of Ito et al. [62]. In parallel flow fields, the two-phase flow regime is bubbly from the inlet to the outlet. In contrast, the twophase flow in the serpentine channels transitions from bubbly to slug flow, increasing the bubble size that partially hinders the supply of

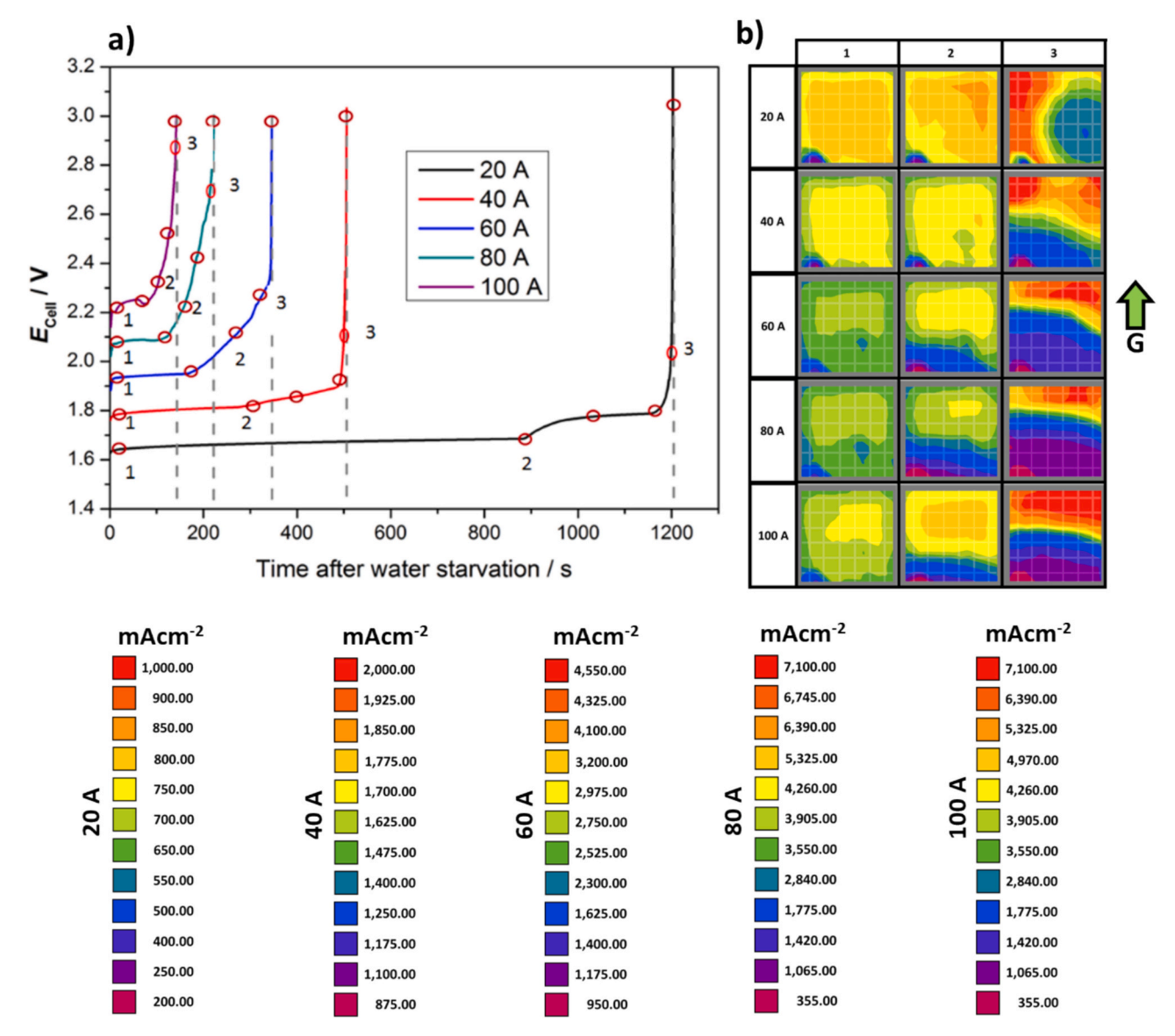


Fig. 4. a) Cell voltage ( $E_{cell}$ ) evolution with respect to time (t) for studying the water/gas distribution in the MEA when operating under low water level conditions. b) current distribution charts at different times and current densities. The experiment simulates the operation of a large-area electrolyzer under high overload conditions (high H2 production rate). Anode flow field: parallel. Cathode flow field: 3-channel serpentine. The feed water enters at the bottom left and exits at the top right on the cathode side. The corresponding color code scales are shown on the bottom.

reactant water to the electrode and increases the mass transport losses along the channels [41,46,62]. This finding is confirmed by the EIS measurement displayed in the Nyquist plot in Fig. 5 b). EIS curves are recorded at 0.2, 0.5 and 1 A cm<sup>-2</sup>. The EIS curves of the parallel flow field always follow the shape of a single arc. In contrast, the impedance curve of the serpentine flow field consists of three arcs. Furthermore, the left intersection is shifted to the right, indicating that high ohmic resistance values are present for the serpentine flow field. As assumed earlier, when the serpentine flow field is used, gas is not removed effectively, worsens the contact of the active area. The definitions of different arcs are controversial in the community. The high-frequency arc is often assigned to charge transfer constrictions and to the hydrogen evolution reaction (HER) [57,58]. Elsøe et al. hypothesized that the middle frequency arc can be ascribed to the oxidation process of Ir<sup>IV</sup> to Ir<sup>V</sup> and the low frequency arc to the oxidation process of Ir<sup>V</sup> to Ir<sup>VI</sup> [58]. Lettenmeier et al. assigned the second arc to the charge transfer process and the third arc to mass transport phenomena [57]. Our measurements favor the assignment to mass transfer, as oxidation processes are not influenced by the flow field design. These results highlight the

abilities of SBPPs to study and characterize new components and designs with respect to mass transport restrictions with local resolution.

This knowledge is used for investigations at high current densities. When the current values or the active area exceed a certain quantity, standard EIS devices reach their measurement limits. Therefore, in this series of experiments, we investigate the use of SBPP for the detection of in situ mass transport limitations at high current densities. Fig. 6 a) shows that the forward and backward polarization curves reach 5.5 A cm<sup>-2</sup>. At low current densities, the curve has almost no visible hysteresis; however, it becomes more pronounced when the current is increased. The occurrence of hysteresis indicates mass transport losses [57]. The potentiostat used in this work (Zahner-Elektrik GmbH & Co. KG, PP241 PowerPotentiostat) can measure up to 1 Acm<sup>-2</sup>, which is plotted in the insets in Fig. 6 a) along with the results for 0.1 and 0.5 A cm<sup>-2</sup>. As expected, no second arc and thus no mass transport losses are visible in this Nyquist plot for these current densities since hysteresis occurs at high currents. Small differences in the left intersection can be attributed to the local temperature increase within the cell, reducing the ohmic resistance values. The CDD for the upward curve 1) in Fig. 6 b)

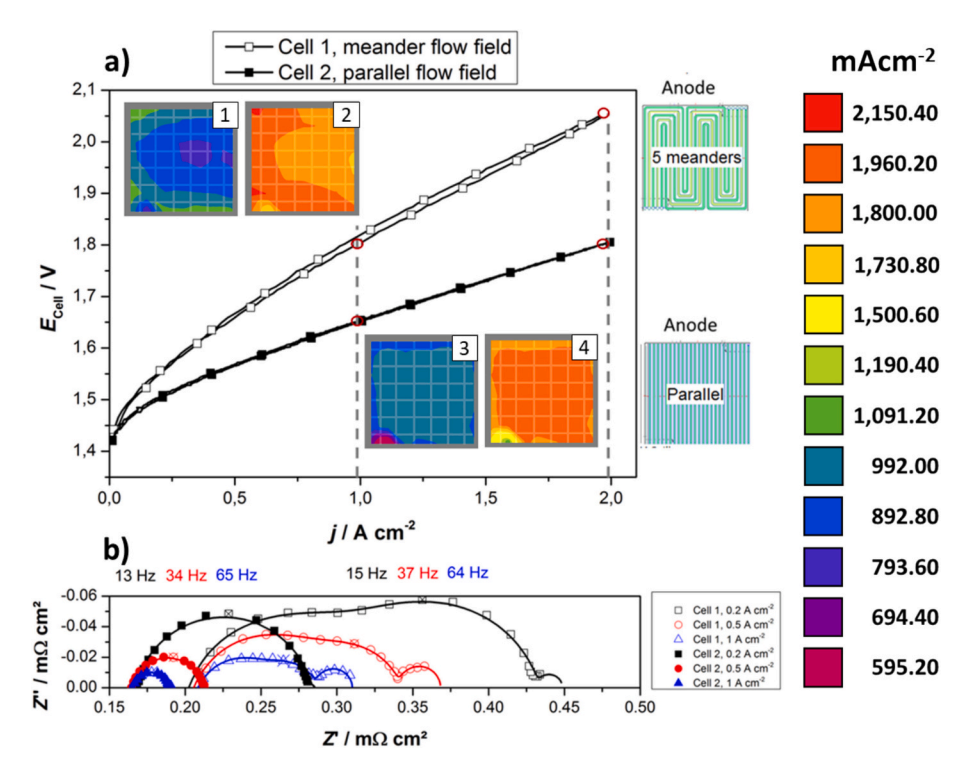
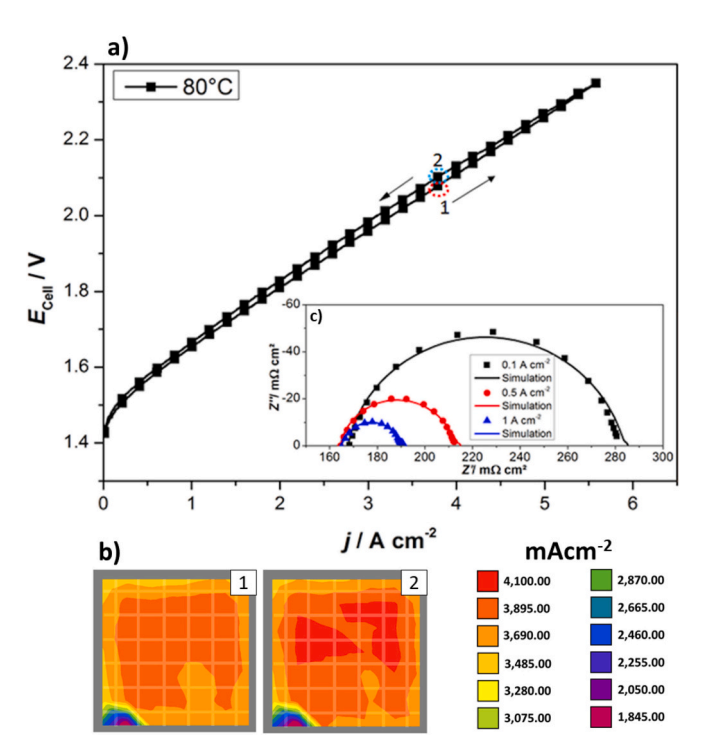


Fig. 5. a) Cell voltage ( $E_{cell}$ ) vs. current density (j) from cells with two different anode flow fields: empty symbols indicate 5-channel serpentine and filled symbols indicate parallel (schemes on the right). The current distribution charts are presented in the plot at 1) and 3) at 1 A cm<sup>-2</sup> and 2) and 4) at 2 A cm<sup>-2</sup>. The color code of the current density is shown on the right. b) Nyquist plots of the EIS measurements at 0.2, 0.5 and 1 A cm<sup>-2</sup>. The apex of the frequency is indicated. The feed water enters at the bottom left and exits at the top right on the cathode side.



**Fig. 6.** a) Cell voltage ( $E_{cell}$ ) vs. current density (j) curves up to 5.5 A cm $^{-2}$ . The inset presents the Nyquist diagrams of the EIS measurements at 0.1, 0.5 and 1 A cm $^{-2}$ . b) The corresponding current density distribution charts at 4 A cm $^{-2}$  for the (1) forward and (2) backward scans. The color code of the current density is shown on the right. Anode flow field: parallel. Cathode flow field: 3-channel serpentine. The feed water enters at the bottom left and exits at the top right on the cathode side.

shows a uniformly distributed current density, while it is more heterogeneous for the downward curve 2). In the upper part of the cell, the current density is noticeably increased when going from high to low current. The measured CDD in 2) shows a similar distribution as at the beginning of the water shortage in Fig. 4 b). Since a lack of water can be excluded due to a high water flow rate, the causes of the variations in the current mapping can be attributed to mass transport phenomena due to the increased gas production and poor gas removal. These results correspond to the course of the polarization curve and the measured hysteresis.

Thus, this series of experiments demonstrates that mass transport phenomena can be detected by means of SBPP during operation. This finding indicates the possible use of SBPP for the characterization of cells and stacks at high current densities in R&D and especially as an in situ diagnostic tool for the online detection of mass transport phenomena in commercial stacks and applications.

#### 3.4. Degradation due to CCM poisoning

The complexity of the degradation mechanisms within electrolyzer cells makes it necessary to perform studies with local consideration within the cells. The applicability of SBPP for such purposes is investigated in this experiment. Therefore, the cell is operated for three days without refreshing the water. The CDD values after 1 a), 2 b) and 3 c) days are shown in Fig. 7. The most obvious change is that the current density in the part of the cell circled in red in Fig. 7 a) to c) decreases significantly during this time.

The relative intensity of Ni in the cross section of the CCM is measured by EDS and is shown in Fig. 7 e). The Ni impurities are transported to the membrane by the water on the anode side, diffusing through the membrane and reaching the cathode side. Thus, the intensity of Ni is highest on the anode side of the membrane, and it decreases toward the center; however, it is still noticeable before the intensity on the cathode side increases again. This result is in good

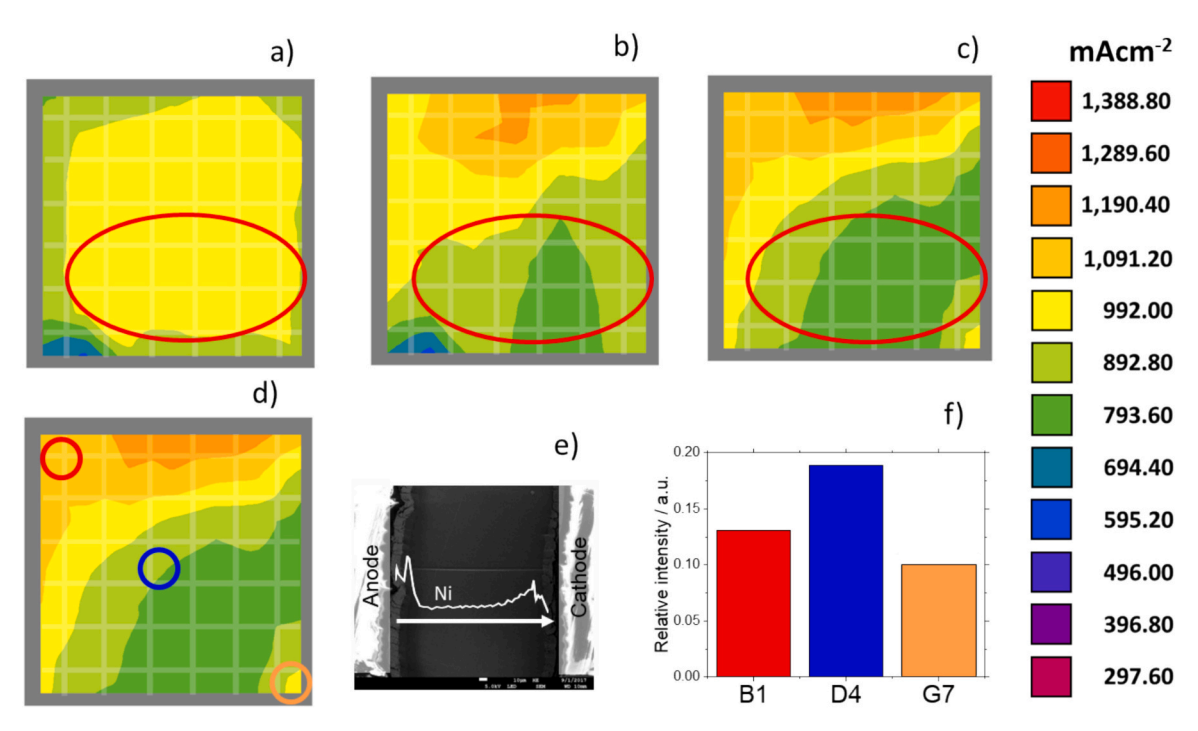


Fig. 7. Current distribution charts after a) one, b) two and c) three days of operation without refreshing the water; thus, the level of Ni impurities increases rapidly. The red ellipse highlights the segments that changed in color, indicating a decrease in the applied current. d) Same chart as c) indicating the zones of the CCM analyzed by EDS: Segments B1, D4, and G7. Relative intensity of the Ni signal in the e) cross section of the electrode (line scan) and f) membrane. Anode flow field: 5-channel serpentine flow field. Cathode flow field: 3-channel serpentine. The feed water enters at the bottom left and exits at the top right on the cathode side. The color code of the current density is shown on the right. (For interpretation of the references to color in this figure legend, the reader is referred to the web version of this article.)

agreement with the reports of Sun et al. [63], who found a similar distribution of contaminants along the CCM cross section.

To verify that the local changes in the CDD are caused by Ni impurities, three areas are defined using the CDD, and their relative intensity is measured by EDS, as displayed in Fig. 7d). The first segment is B1, marked with a red cycle in the upper left corner. High current density can be measured in this segment. Segment D4, labeled with a blue cycle, represents the area in which the current density decreases significantly during the operating time. The last segment G7 is marked with an orange cycle in the bottom right corner. At this point, the current density increases on the third day of operation. When comparing the measured intensities of Ni impurities of the different spots, a clear trend can be observed. Segments B1 und G7 with high current densities have noticeably lower amounts of Ni impurities than segment D4, where the current density is lower. Thus, based on the EDS results, the loss of CDD can be attributed to Ni poisoning the CCM, which occurs inhomogeneously. This inhomogeneous distribution can be explained after cell disassembly. In the areas with low current densities and high impurities, the Au/Ni coating of the SBPP shows significant corrosion, while the other parts are intact. Most likely, a defect during the coating process or a scratch in this area is the reason for the onset of corrosion.

As shown in Fig. 7 poisoning can lead to lower current densities in affected areas causing other regions to rise accordingly. If the local current density exceeds critical values, it is conceivable that local mass transport loses can occur even if the overall current is within a regular range as a consequence of performance heterogeneity. Sun et al. demonstrated the occurrence of a second semi arc due to poisoning [63], which confirms the assumption that poisoning of the CCM and the associated heterogeneity in current density measured with the SBPP can lead to local mass transport losses.

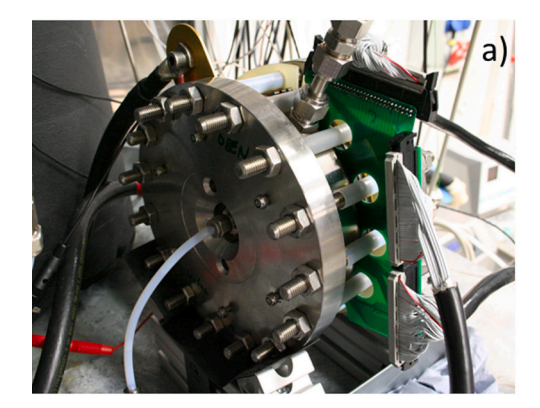
Therefore, by using SBPP, degradation effects can be determined locally, which offers many advantages over the usual measurement of global voltage increase. This demonstrates the use of SBPP to detect degradation caused by unfavorable operating conditions at an early

stage and to initiate countermeasures during operation.

## 3.5. Perspectives of the SBPP in industrial stacks

Laboratory-scale cells are a very efficient method e.g. to investigate degradation phenomena, analyzing the performance of new components or as in this study for first validation of new tools and devices. The implementation of SBPP in commercial stacks could lead to a variety of additional opportunities such as combining in situ diagnosis and online control to avoid critical conditions while maintaining the maximum performance, ensuring homogenous pressure distribution etc. This study was able to demonstrate some of these functions at laboratory-scale cells but upscaling is necessary. Despite the fact that the structure of the segmented cell was designed in such a way that upscaling to larger eletrolyzer is possible, the applicability of the SBPP for PEMWE needs to be evaluated for larger PEMWE stacks. The focus of this study is to demonstrate the versatility of SBPP in general. Nevertheless, a first applicability of the SBPP for PEMWE is evaluated in a short stack from an industrial H<sub>2</sub> generator. The stack is equipped with a prototype SBPP, shown in Fig. 1e), that is specifically designed for this hardware and operated using a commercially available industrial balance of the plant, as shown in Fig. 8 a).

With the given limitations of the industrial system, the specific scenario of feed water shortage is chosen to test the functionality of the SBPP, similar to the single-cell experiment in Section 3.2. The preheated and water-circulated stack is cut from the water supply to provoke local water shortages and thus deactivate the electrolysis process. The frame of the current density map in Fig. 8 b) is recorded at a timestamp of 77 s after startup. The false color plot (purple/blue: low current density, orange/red: high current density) coarsely resembles the circular cross section of the SBPP and the electrolyzer in upright orientation, and it shows interpolated current densities. A high-current density spot in the lower middle area is obvious; the upper third part of the area has a low current density that is <25 % the magnitude of the hot spot current



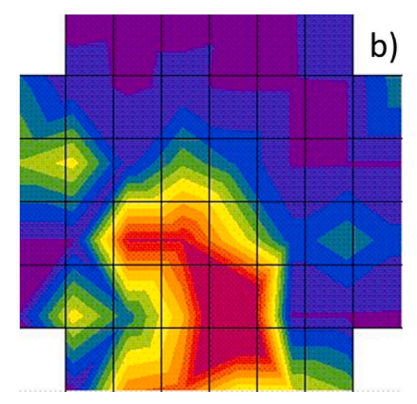


Fig. 8. a) 50 bar electrolysis short stack (EWII Fuel Cells) with segmented BPP and b) current distribution mapping.

density. The water shortage has already led to a local reactant shortage in the upper areas, where product gas accumulates and streams toward the outlet. The principal functionality to record the current density locally is visualized in the plot, and the local resolution can be estimated to be within the range of one segment, as the gradients between two neighboring segments from red to blue cover almost the entire data range. The results are in good agreement with those obtained in laboratory single cells. This strongly suggests that the SBPP is suitable for commercial PEMWE stacks, although further studies and investigations are necessary for verification.

#### 4. Conclusion

An SBPP for current density mapping was developed by adapting the DLR-patented PCB used in PEMFC to PEMWE. The integration of this SBPP enabled online current mapping and thus represented a powerful in situ diagnostic tool. For this study, an SBPP with an area of  $50.2 \times 50.2 \, \mathrm{mm}^2$  divided into 49 segments was manufactured. To demonstrate its versatility, SBPP was integrated into a single cell. Several experiments simulating real operating conditions were conducted. Current mapping varied considerably, which was attributed to the different conditions and verified by the polarization curves and EIS measurements.

With the SBPP, the general loss of clamping pressure could be shown, and the positions could be determined. Inhomogeneities in temperature over the cell area could not be observed. However, the tool was very useful for studying gas/water management, inadequate flow field designs in the BPP and mass transport losses at high current densities. The most important advantage of the segmented cell was for studying local degradation due to impurities in the water. Thus, this diagnostic method was an important addition to study PEMWE during operation.

A conceivable integrability in research or commercial stacks would open further application possibilities such as combining in situ diagnosis and online regulation to avoid critical conditions but further studies are necessary.

Overall, the wide variety of experiments performed in this work demonstrated the versatility and advantages of using SBPP in many different research fields. Among other things, SBPP can be used for designing and developing components for operation at high current densities and for studying mass transport phenomena [64]; additionally, it can be used to investigate the effect of membrane poisoning by corrosion products during long-term tests on stacks e.g. with stainless steel components [65]. Therefore, the segmented cell is a very useful diagnostic tool in PEMWE for monitoring and analyzing local phenomena.

## **Funding**

The research leading to these results was funded by the European

Union's Seventh Framework Programme (FP7/2007–2013) for Fuel Cell and Hydrogen Joint Technology Initiative under Grant No. 621237 (INSIDE).

#### CRediT authorship contribution statement

Benjamin Kimmel: Writing – original draft, Methodology, Investigation, Conceptualization. D. Garcia-Sanchez: Visualization, Validation, Investigation, Conceptualization. T. Morawietz: Visualization, Formal analysis. M. Schulze: Visualization, Investigation. I. Biswas: Visualization, Investigation. A.S. Gago: Supervision, Conceptualization. K.A. Friedrich: Supervision.

### **Declaration of competing interest**

The authors declare that they have no known competing financial interests or personal relationships that could have appeared to influence the work reported in this paper.

#### Appendix A. Supplementary data

Supplementary data to this article can be found online at  $\frac{\text{https:}}{\text{doi.}}$  org/10.1016/j.apenergy.2024.125106.

#### Data availability

The data that has been used is confidential.

## References

- European Commission. A hydrogen strategy for a climate-neutral Europe. Brussels: European Commission; 2020.
- [2] European Commission, "eurostat, "European Commission, [Online]. Available, https://ec.europa.eu/eurostat/web/energy/data/database [Zugriff am 17.08.2022].
- [3] Umwelt Bundesamt [Online]. Available, https://www.umweltbundesamt.de/en/image/renewable-energy-share-in-gross-final-energy [Zugriff am 17.08.2022].
- [4] Barnhart CJ, Dale M, Brandt AR, Benson SM. The energetic implications of curtailing versus storing solar- and wind-generated electricity. Royal Society of Chemistry 2013. https://doi.org/10.1039/C3EE41973H.
- [5] Smolinka T, Ojong ET, Garche J. Hydrogen production from renewable energies -Electrolyzer technologies, in electrochemical energy storage for renewable sources and grid balancing. Elsevier 2014. https://doi.org/10.1016/B978-0-444-62616-5.00008-5.
- [6] Lettenmeier P, Wang R, Abouatallah R, Burggraf F, Gago AS, Friedrich KA. Coated stainless steel bipolar plates for proton exchange membrane Electrolyzers. J Electrochem Soc 2016:163(11).
- [7] Kang Z, Mo J, Yang G, Li Y, Talley DA, Han B, et al. Performance modeling and current mapping of proton exchange membrane Electrolyzer cells with novel thin TunableL iquid gas diffusion layers. Electrochim Acta 2017;255. https://doi.org/ 10.1016/j.electacta.2017.09.170
- [8] Kang Z, Mo J, Yang G, Li Y, Talley DA, Zhang FY, et al. Investigation of Pore Shape Effects of Novel Thin LGDLs for High-Efficiency Hydrogen/Oxygen Generation and Energy Storage, 15th International Energy Conversion Engineering Conference. 2017. https://doi.org/10.1016/j.electacta.2017.09.170.

- [9] Steen SM, Mo J, Kang Z, Yang G, Zhang F-Y. Investigation of titanium liquid/gas diffusion layers in proton exchange membrane electrolyzer cells. International Journal of Green Energy 2017;14. https://doi.org/10.1080/ 15435075 2016 1253582
- [10] Lettenmeier P, Kolb S, Burggraf F, Gago AS, Friedrich KA. Towards developing a backing layer for proton exchange membrane Electrolyzers. J Power Sources 2016; 311. https://doi.org/10.1016/j.jpowsour.2016.01.100.
- [11] Lettenmeier P, Wan R, Saruhan RAB, Freitag O, Gazdzicki P, Morawietz T, et al. Low-cost and durable bipolar plates for proton exchange membrane Electrolyzers, scientific reports 7. Article number 2017;44035. https://doi.org/10.1038/ srep44035.
- [12] Biswas I, Sánchez DG, Schulze M, Mitzel J, Kimmel B, Gago AS, et al. Advancement of segmented cell Technology in low Temperature Hydrogen Technologies. Energies 2020. https://doi.org/10.3390/en13092301.
- [13] Cleghorn SJC, Derouin CR, Wilson MS, Gottesfeld S. A printed circuit board approach to measuring current distribution in a fuel cell. J Appl Electrochem 1998; 28. https://doi.org/10.1023/A:1003206513954.
- [14] L. Perez, L. Brandao, J. Sousa und A. Mendes, "Segmented polymer electrolyte membrane fuel cells - A review", Renewable and Sustainable Energy Reviews, Elsevier. Volume 15.
- [15] Stumper J, Campbell S, Wilkinson D, Johnson M, Davis M. In-situ methods for the determination of current distributions in PEM fuel cells. Electrochim Acta 1998;14. https://doi.org/10.1016/S0013-4686(98)00137-6.
- [16] Noponen M, Mennola T, Mikkola M, Hottinen T. Measurement of current distribution in a free-breathing PEMFC. J Power Sources 2002;106. https://doi. org/10.1016/S0378-7753(01)01063-1.
- [17] Yoon YG, Lee WY, Yang TH, Park GG, Kim CS. Current distribution in a single cell of PEMFC. J Power Sources 2003;118. https://doi.org/10.1016/S0378-7753(03) 00003.4
- [18] Hwnag J, Chang W, Peng R, Chen P, Su A. Experimental and numerical studies of local current mapping on a PEM fuel cell. Int J Hydrog Energy 2008;33. https:// doi.org/10.1016/j.ijhydene.2008.07.035.
- [19] Schulze M, Gulzow E, Schönbauer S, Knöri T, Reissner R. Segmented cells as tool for development of fuel cells and error prevention/prediagnostic in fuel cell stacks. J Power Sources 2007;173. https://doi.org/10.1016/j.jpowsour.2007.03.055.
- [20] Lin R, Sander H, Gülzow E, Friedrich AK. Investigation of locally resolved current density distribution of segmented PEM fuel cells to detect malfunctions. ECS Trans 2010;26. https://doi.org/10.1149/1.3428993.
- [21] Sanchez DG, Ortiz A, Friedrich K. Oscillation of PEFC under low cathode humidification: effect of gravitation and bipolar plate design. J Electrochem Soc 2013;160. https://doi.org/10.1149/2.091306jes.
- [22] Sanchez DG, Ruiu T, Friedrich KA, Sanchez-Monreal J, Vera M. Analysis of the influence of temperature and gas humidity on the performance stability of polymer electrolyte membrane fuel cells. J Electrochem Soc 2016;163. https://doi.org/ 10.1149/2.0071603jes.
- [23] García-Salaberri P, Sanchez D, Boillat P, Vera M, Friedrich K. Hydration and dehydration cycles in polymer electrolyte fuel cells operated with wet anode and dry cathode feed: a neutron imaging and modeling study. J Power Sources 2017; 359. https://doi.org/10.1016/j.jpowsour.2017.03.155.
- [24] Reshetenko T, Bender G, Bethune K, Rocheleau R. Systematic studies of the gas humidification effects on spatial PEMFC performance distributions. Electrochim Acta 2012;69. https://doi.org/10.1016/j.electacta.2012.02.111.
- [25] Sanchez DG, Ruiu T, Biswas I, Schulze M, Helmly S, Friedrich KA. Local impact of humidification on degradation in polymer electrolyte fuel cells. J Power Sources 2017;352. https://doi.org/10.1016/j.jpowsour.2017.03.057.
- [26] Reshetenko TV, St-Pierre J. Study of acetylene poisoning of Pt cathode on proton exchange membrane fuel cell spatial performance using a segmented cell system. J Power Sources 2015;287. https://doi.org/10.1016/j.jpowsour.2015.04.073.
- [27] Liang D, Shen Q, Hou M, Shao Z, Yi B. Study of the cell reversal process of large area PEMFC under fuel starvation. J Power Sources 2009;194. https://doi.org/ 10.1016/j.jpowsour.2009.06.059.
- [28] Dou M, Hou M, Shen Q, Znahg H, Lu W, Shao Z, et al. Behaviors of PEMFC under oxidant starvation. J Power Sources 2011;196. https://doi.org/10.1016/j. ipowsour.2010.11.005.
- [29] Baumann N, Blankenship A, Dorn M, Cremers C. Evaluating current distribution and influence of defect sites for graphitic compound bipolar plate materials. Fuel Cells 2019. https://doi.org/10.1002/fuce.201900138.
- [30] Liu Z, Yang L, Mao Z, Zhuge W, Zhang Y, Wang L. Behavior of PEMFC in starvation. J Power Sources 2006;157. https://doi.org/10.1016/j.jpowsour.2005.08.006.
- [31] Reshetenko TV, Benderb G, Bethune K, Rochele R. Systematic study of back pressure and anode stoichiometry effects on spatial PEMFC performance distribution. Electrochim Acta 2011;56. https://doi.org/10.1016/j. electacta.2011.07.058.
- [32] Reshetenko T, Bender G, Bethune K, Rocheleau R. Effects of local variations of the gas diffusion layer properties on PEMFC performance using a segmented cell system. Electrochim Acta 2012;80. https://doi.org/10.1016/j. electacta.2012.07.031.
- [33] Kaz T, Sander H, Schönbauer S. Device for measuring local current/heat distribution on electrochemical electrode has current flow direction to resistance element transverse to current flow direction to current conducting element. Patent 2004;DE10316117 B3.
- [34] Kaz T, Sander H, Schönbauer S. Measurement of the current distribution/heat distribution of an electrochemical electrode. Patent 2006;EP1618395 A1.
- [35] Reshetenko T, St-Pierre J, Rocheleau R. Effects of local gas diffusion layer gas permeability variations on spatial proton exchange membrane fuel cells

- performance. J Power Sources 2013;241. https://doi.org/10.1016/j.jpowsour.2013.04.131.
- [36] Lin R, Gülzow E, Schulze M, Friedrich KA. Investigation of membrane pinhole effects in polymer electrolyte fuel cells by locally resolved current density. J Electrochem Soc 2010;158. https://doi.org/10.1149/1.3504255.
- [37] Reshetenko T, Bender G, Bethuneund K, Rocheleau R. Application of a segmented cell setup to detect pinhole and catalyst loading defects in proton exchange membrane fuel cells. Electrochim Acta 2012;76. https://doi.org/10.1016/j. electacta 2012 04 138
- [38] Martinez-Vazquez B, Sanchez D, Castillo J, Friedrich K, Garcia-Ybarra P. Scaling-up and characterization of ultralow-loading MEAs made-up by electrospray. Int J Hydrog Energy 2015;40. https://doi.org/10.1016/j.ijhydene.2015.01.111.
- [39] I. Biswas, D. G. Sanchez und M. Schulze, Operando monitoring of local current density distributions in PEMWE, AWE and AEMWE, in European Hydrogen Energy Conference 2018, Malaga, Spanien, 2018.
- [40] Wallnofer-Ogris E, Grimmer I, Ranz M, Hoglinger M, Kartusch S, Rauh J, et al. A review on understanding and identifying degradation mechanisms in PEM water electrolysis cells: insights for stack application, development, and research. Int J Hydrog Energy 2024;65. https://doi.org/10.1016/j.ijhydene.2024.04.017.
- [41] Merwe JVD, Uren K, Schoorund GV, Bessarabov D. Characterisation tools development for PEM electrolysers. Int J Hydrog Energy 2014;39. https://doi.org/ 10.1016/j.ijhydene.2014.02.096.
- [42] Dedigama I, Angeli P, Dijk NV, Millichamp J, Tsaoulidis D, Shearingund PR, et al. Current density mapping and optical flow visualisation of a polymer electrolyte membrane water electrolyser. J Power Sources 2014;265. https://doi.org/ 10.1016/j.jpowsour.2014.04.120.
- [43] Sun S, Xiao Y, Liang D, Shao Z, Yu H, Hou M, et al. Behaviors of a proton exchange membrane electrolyzer under water starvation. RSC Adv 2015. https://doi.org/ 10.1039/C4RA14104K.
- [44] Immerz C, Schweins M, Trinke P, Bensmann B, Paidar M, Bystroň T, et al. Experimental characterization of inhomogeneity in current density. Electrochim Acta 2017;260. https://doi.org/10.1016/j.electacta.2017.12.087.
- [45] Immerz C, Bensmann B, Trinke P, Suermann M, Hanke-Rauschenbach R. Local current density and electrochemical impedance measurements within 50 cm Single-Channel PEM electrolysis cell. J Electrochem Soc 2018;165. https://doi.org/ 10.1149/2.0411816jes.
- [46] Minnaar C, Beer FD, Bessarabov D. Current density distribution of Electrolyzer flow fields in SituCurrent mapping and neutron radiography. Energy Fuel 2020. https:// doi.org/10.1021/acs.energyfuels.9b03814.
- [47] Verdin B, Fouda-Onana F, Germe S, Serre G, Jacques P, Millet P. Operando current mapping on PEM water electrolysis cells. Influence of mechanical stress. Int J Hydrog Energy 2017;42. https://doi.org/10.1016/j.ijhydene.2017.08.189.
- [48] Al Shakhshir S, Zhou F, Kær SK. On the effect of clamping pressure and methods on the current distribution of a proton exchange membrane water Electrolyzer. ECS Trans 2018;85(13). https://doi.org/10.1149/08513.0995ecst.
- [49] Parra-Restrepo J, Bligny R, Dillet J, Didierjean S, Stemmelen D, Moyne C, et al. Influence of the porous transport layer properties on the mass and charge transfer in a segmented PEM electrolyzer. Volume 2020;65. https://doi.org/10.1016/j. iihvdene.2020.01.100.
- [50] Roenning FH, Roy A, Aaron DS, Mench MM. Mass transport limitations in polymer electrolyte water electrolyzers using spatially-resolved current measurement.
   Volume 2022;542. https://doi.org/10.1016/j.jpowsour.2022.231749.
   [51] Hensle Niklas, Metz Sebastian, Weber André, Smolinka Tom. A segmented along
- [51] Hensle Niklas, Metz Sebastian, Weber André, Smolinka Tom. A segmented along the channel test cell for locally resolved analysis at high current densities in PEM water electrolysis. J Electrochem Soc 2024;171(11). https://doi.org/10.1149/ 1945-7111/ad9064.
- [52] Wang K, Xu C, Xiao F, Zhang T, Ta L, Ma S, et al. Operando analysis of in-plane heterogeneity for the PEM electrolyzer cell: mappings of temperature and current density. Volume 2024;436. https://doi.org/10.1016/j.jclepro.2024.140586.
- [53] Garcia-Navarro JC, Schulze M, Friedrich KA. "measuring and modeling mass transport losses in proton ex-change membrane water electrolyzers using electrochemical impedance spectroscopy", journal of power sources 431. Elsevier 2019. https://doi.org/10.1016/j.jpowsour.2019.05.027.
- [54] Navarro Julio César García. On the mass transport phenomena in proton exchange membrane water electrolyzers. doctoral dissertation,. University of Stuttgart; 2020. https://elib.uni-stuttgart.de/handle/11682/11046.
- [55] Siracusano S, Baglio V, Grigoriev S, Merlo L, Fateev V, Arico A. The influence of iridium chemical oxidation state on the performance and durability of oxygen evolution catalysts in PEM electrolysis. J Power Sources 2017;366. https://doi.org/ 10.1016/j.jpowsour.2017.09.020.
- [56] Nie J, Chen Y, Boehm RF, Katukota S. A Photoelectrochemical model of proton exchange water electrolysis for hydrogen production. J Heat Transf 2008;130. https://doi.org/10.1115/1.2789722.
- [57] Lettenmeier P, Kolb S, Sata N, Fallisch A, Zielke L, Thiele S, et al. Comprehensive investigation of novel pore-graded gas diffusion layers for high-performance and cost-effective proton exchange membrane electrolyzers. Energy Environ Sci 2017. https://doi.org/10.1039/C7EE01240C.
- [58] Elsøe K, Grahl-Madsen L, Scherer G, Hjelm J, Mogensen MB. Electrochemical characterization of a PEMEC using impedance spectroscopy. J Electrochem Soc 2017;164. https://doi.org/10.1149/2.0651713jes.
- [59] Anderson E, Ayers K, Capuano C. "R&D Focus Areas Based on 60,000 hr Life PEM Water Electrolysis Stack Experience PEM Water Electrolysis Stack Experience", First International Workshop on Durability and Degradation Issues in PEM Electrolysis Cells and its Components, Freiburg, Germany, 2013. Available online, https://www.sintef.no/globalassets/project/novel/pdf/1-1\_proton\_everett\_public.pdf (accessed on 26 July 2022).

- [60] "Hydrogen: The next generation. Discover Cummins electrolyzer technologies", Available online, https://mart.cummins.com/imagelibrary/data/assetfiles/00 71313.pdf (accessed on 26 July 2022).
- [61] SILIYER 300-Die Nächste Dimension der PEM-Elektrolyse", Available online, https://assets.new.siemens.com/siemens/assets/api/uuid:abae9c1e48d6d239c06d88e 565a25040ed2078dc/version:1524040818/ct-ree-18-047-db-silyzer-300-db-de-en-rz.pdf (accessed on 26 July 2022).
- [62] Ito H, Maeda T, Nakano A, Hasegawa Y, Yokoi N, Hwang CM, et al. Effect of flow regime of circulating water on a proton exchange membrane electrolyzer. Int J Hydrog Energy 2010;35. https://doi.org/10.1016/j.ijhydene.2010.06.103.
- [63] Sun S, Shao Z, Yu H, Li G, Yi B. Investigations on degradation of the long-term proton exchange. J Power Sources 2014;267. https://doi.org/10.1016/j. jpowsour.2014.05.117.
- [64] Stiber S, Balzer H, Wierhake A, Wirkert FJ, Roth J, Rost U, et al. Porous transport layers for proton exchange membrane electrolysis under extreme conditions of current density, temperature, and pressure. Adv Energy Mater 2021;11. https:// doi.org/10.1002/aenm. 202100630.
- [65] Stiber S, Hehemann M, Carmo M, Müller M, Ayers KE, Capuano C, et al. Long-term operation of Nb-coated stainless steel bipolar plates for proton exchange membrane water Electrolyzers. Adv Energy Mater 2022;3. https://doi.org/10.1002/ aesr.202200024.